doi:10.2533/chimia.2022.529 Chimia 76 (2022) 529–537

Ultrafast Single-particle Imaging with Intense X-ray Pulses

Zhibin Sun[a], Andre Al Haddad[a], Sven Augustin[a], Gregor Knopp[a], Jonas Knurr[a], Kirsten Schnorr[a], and Christoph Bostedt[a,b*]

Abstract: Ultrafast single-particle imaging with intense x-ray pulses from free-electron laser sources provides a new approach for visualizing structure and dynamics on the nanoscale. After a short introduction to the novel free-electron laser sources and methods, we highlight selected applications and discuss how ultrafast imaging flourishes from method development to early applications in physics and biology to opportunities for chemical sciences.

Keywords: Ultrafast imaging · Free-electron laser · X-ray

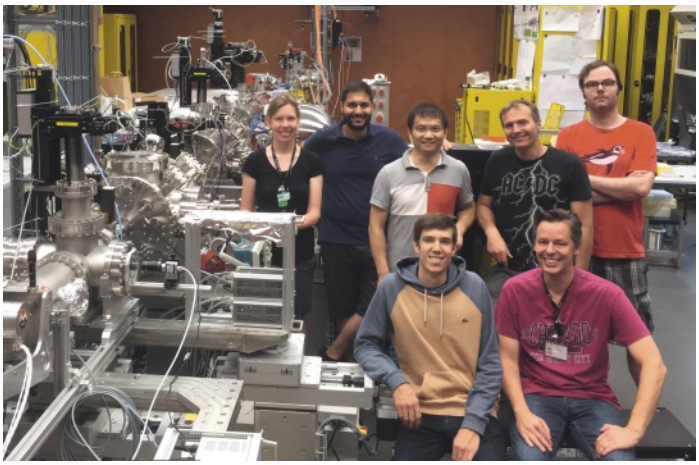

The Maloja team at SwissFEL. Standing from left to right: Kirsten Schnorr, Andre Al Haddad, Zhibin Sun, Gregor Knopp, and Sven Augustin. Seated from left to right: Jonas Knurr and Christoph Bostedt. The team started with the Maloja endstation project in 2019. The endstation received first light in 2020 and the first call for user proposals was published in 2021. The Maloja endstation provides many opportunities for ultrafast chemistry, non-linear x-ray sciences, and single-particle imaging.

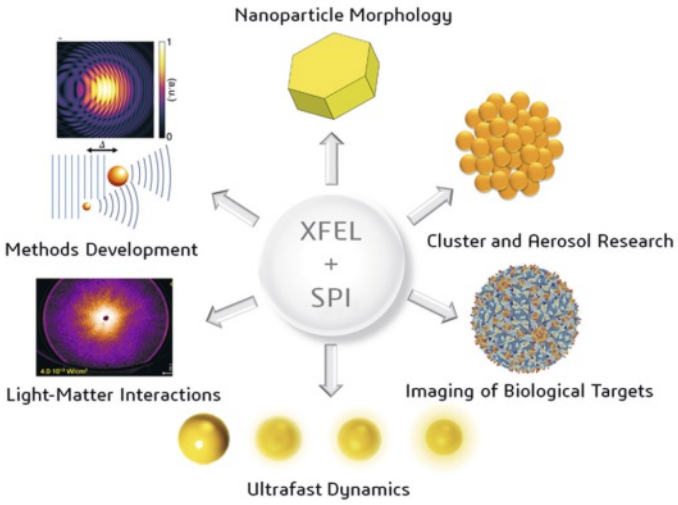

Fig. 1. Ultrafast single-particle imaging revolves around fundamental light-matter interactions to methods development to applications in nanoscale research and ultrafast dynamics.

1. Introduction

Imaging, that is the visualization of objects or processes, is undoubtably one of the central tools in natural sciences. The attainable resolution is directly related to the employed wavelengths and x-rays are ideally suited to get a glimpse into the nanoworld. Equally important is the exposure time or shutter speed that determines the time resolution with which dynamic processes can be followed. The intense and coherent x-ray pulses from x-ray free-electron lasers (XFELs) have inspired new approaches and opened opportunities for visualizing dynamics and transient states in single, nanometer-sized particles in a single shot. Since the first short-wavelength FELs became operational,[1] this field has rapidly developed and imaging as well as diffraction techniques have been developed for various applications.

The fundamental approach in ultrafast imaging is that an intense, femtosecond x-ray pulse is focused on the sample, generating a diffraction image which is recorded in one instance. The sample will be destroyed during the process, but the image is recorded prior to the sample explosion. This approach is commonly referred to as the "diffract before destroy" method.[2] Many of the early experiments focused on the fundamental light-matter interaction and ultrafast sample damage to confirm the validity of the diffract before destroy approach.[3] In the last decade an increasing number of method developments and ultrafast imaging applications have flourished at XFELs at the intersection of physical, biological, and chemical sciences.[4] In this article, we will give a short introduction to XFELs with a focus on the SwissFEL facility at the Paul-Scherrer-Institute. We will then describe the experimental approaches for single-shot single-particle experiments and present representative scientific applications as well as current developments for imaging ultrafast dynamics and

*Correspondence: Prof. Dr. C. Bostedt, E-mail: christoph.bostedt@psi.ch [a]Paul Scherrer Institut (PSI), 5232 Villigen PSI [b]LUXS Laboratory for Ultrafast X-ray Sciences, Ecole Polytechnique Fédérale de Lausanne (EPFL), 1015 Lausanne

electronic structure. We will close with a short description of the growing opportunities for ultrafast imaging experiments at the new SwissFEL Maloja endstation.

2. X-ray Free-electron Lasers

Free-electron lasers are accelerator-based light sources where a small fraction of the kinetic energy of a relativistic electron beam is converted into an intense beam of electromagnetic radiation.[1,4] The key process in a free-electron laser is based on the resonant interaction between the electron bunch and radiation in an undulator as depicted in Fig. 2. In simple terms, the spontaneous emission at the beginning of the undulator imprints its wavelengths onto the electron bunch. Accordingly, the electrons start emitting in phase and the output scales with N^2 for coherent emission compared to N for incoherent emission, with N being the number of electrons in the bunch. The process is called self-amplified spontaneous emission (SASE), where the electron beam microbunching and the radiation power grow as a function of the undulator distance until the process reaches saturation. Compared to an optical laser, in a SASE FEL the electron beam is the energy pump and the lasing medium at the same time. Due to the lack of suitable optics in the x-ray spectral regime, no cavities can be built and therefore all current XFEL are high-gain, single pass lasers.

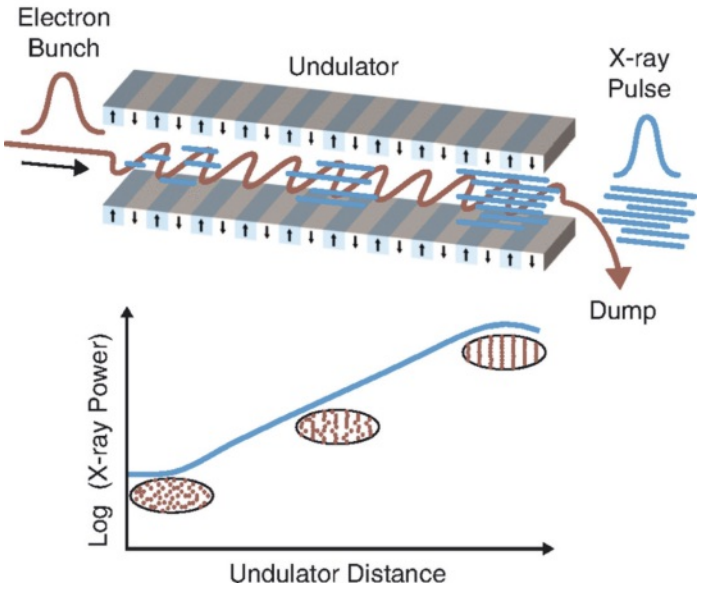

Fig. 2. Principle of the SASE lasing process. The microbunching along the undulator line leads to exponential growth in radiation output. Image reproduced with permission from ref. [4].

Compared to other x-ray sources, FELs deliver orders of magnitudes higher peak brilliances (*c.f.* Fig. 3) and almost fully transversally coherent radiation. As a rule of thumb, the intense x-ray pulses of FELs contain 10^{12} photons in a 100 fs pulse, resulting in high peak powers of tens of gigawatts. The pulse durations range in standard operations typically from hundreds to few tens of emtosecond (fs) and the bandwidth of the emitted x-ray is below 1% of the fundamental energy. Over the past decade, FEL research has witnessed a rapid development and many theoretical concepts have been experimentally implemented and further improved. Selected examples range from the generation of few femtosecond to attosecond pulses[5] to two-color modes for pump / probe experiments.[6,7] The repetition rate of FELs depends on the chosen accelerator technology. FELs based on conventional, "warm" copper cavities operate with repetition rates around 100 Hz whereas superconducting cryogenic accelerators, such as the European XFEL facilities or the upgraded LCLS-II in Stanford (USA) can support repetition rates from tens of kHz to MHz.

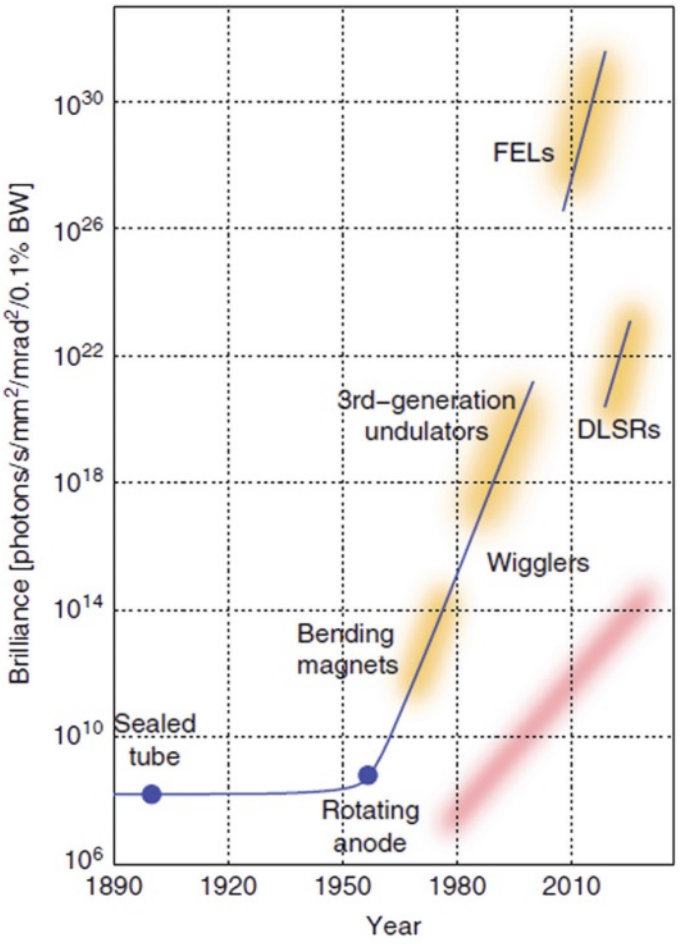

Fig. 3. Growth of the brilliance of x-ray sources over time. The red line indicates the famous Moores law for growth of integrated circuits for comparison. Image reproduced with permission from ref. [8].

The Swiss free-electron laser SwissFEL is based on a compact design concept capable of lasing at 1 Å, but with investment and operation costs substantially reduced in comparison with other facilities of similar scientific potential.[9] A special feature of SwissFEL is that two bunches, separated by 28 ns but in the same RF macropulse, can be accelerated and then separated with a fast kicker into two undulator lines, see Fig. 4, allowing full parallel operations of two FEL lines. The Aramis hard x-ray line can deliver photon energies from 2 keV to 14.4 keV and the Athos soft x-ray line can deliver photon energies from 0.25 keV to 1.8 keV. The Athos branch includes a novel layout of alternating magnetic chicanes and short undulator segments. Together with the APPLE X architecture of undulators, the Athos branch can be operated in different modes producing FEL beams with special characteristics ranging from attosecond pulse length to high power modes.[10,11]

2.1 *Experimental Approaches*

Single-particle imaging experiments require in principle only a suitable photon area detector as well as a sample delivery system but the experiments are often combined with further spectrometers (Fig. 5). The photon area detector needs to be synchronized with the XFEL pulses and ideally also supports their full repetition rate. Early experiments at FLASH used a simple, multichannel plate – phosphor stack system to convert the x-ray photons into

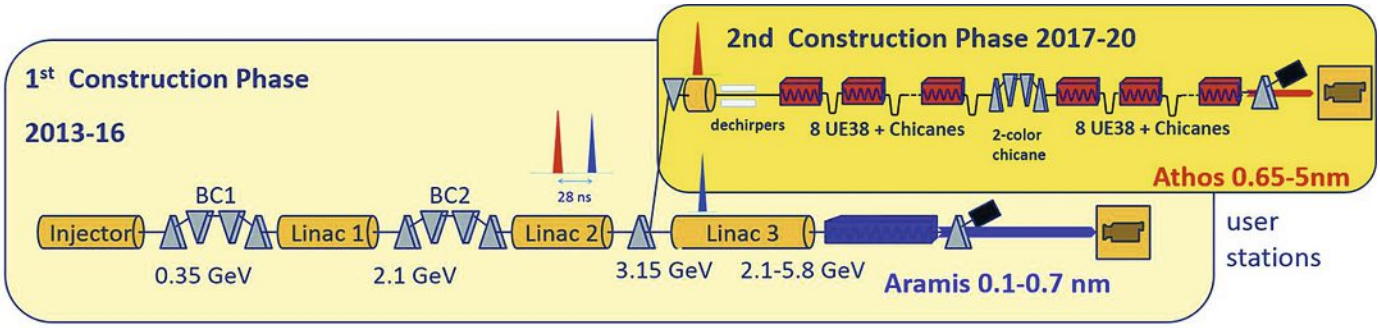

Fig. 4. Schematic of the SwissFEL free-electron laser. After the second accelerator section the bunches are separated and feed both, the Aramis hard x-ray line and Athos soft x-ray line at the full repetition rate. Image reproduced from ref. [11].

visible light and an external camera for data recording.[12] A real breakthrough was the incorporation of in-vacuum pnCCD sensors in the CAMP endstation first used at LCLS[13] and still under use at FLASH and the European XFEL. These detectors exhibit a greatly increased linearity and finer pixel resolution. The energy resolution in each pixel allows to discriminate the elastically scattered photons over inelastically scattered light or plasma emission from the sample target. At SwissFEL, a new generation of pixel detectors are used which feature a slightly higher noise level but a dramatically improved dynamic range per pixel, overcoming some of the earlier limitations in recording the lower order diffraction signals.[14]

For the sample delivery there are two basic approaches, fixed targets on a membrane or free-flying targets. The fixed targets require less sample material and if required the same sample can be investigated under low-fluence conditions with multiple shots.[15] To exploit the advantages of single shot imaging, free flying targets are advantageous. They allow the investigation of samples that would be altered or even destroyed by any interactions with the environment as discussed below. Further, the lack of a support membrane greatly reduces the background signal and opens the door for smaller or weakly scattering samples. Many imaging experiments are performed on van der Waals systems with pulsed supersonic jets[12] or cryogenic continuous expansion sources.[16] For biological samples and more recently also colloidal nanoparticles, aerodynamic lens systems with either a gas dynamic virtual nozzle or electrospray source have been optimized for the use in single-particle imaging experiments.[17] A third possibility is that existing sample sources such as for example metal cluster sources are adapted to the FEL endstations.[18]

An approach that has proven very useful is to complement the imaging setup with spectrometers for coincident imaging and spectroscopy.[19] Most commonly ion time-of-flight spectrometers are integrated as depicted in Fig. 5. The correlation of both data, taken within the same few femtosecond x-ray pulse, yields additional information about the sample position in the focal volume,[19] the composition of core-shell structures,[20] or aerosols,[21] or it can be simply taken as a hit finder as often the free-flying particle experiments exhibit hit rates far below 10%.

We want to conclude with a short note about the data management. For single-particle imaging experiments at FELs, each shot on the target is a complete experiment. Therefore all devices entering the data stream have to be carefully synchronized which is typically achieved by the FEL facility with an extensive synchronization and data management scheme. At the same time, the experiments produce many Megabyte of data at the repetition rate of the machines which are currently in the hundreds of Hertz and soon Kilo-Hertz regime. Accordingly, full single-particle imaging data sets reach many Terabytes per sample and accordingly require an adequate high-performance computer.

A key difference between x-ray imaging and optical or electron microscopy is that there are no suitable lenses that can transform the signals back from the Fourier into real space. As only the diffraction signal is recorded and as the phase information is lost during the detection process, simple Fourier transforms back into real space are not possible. Simple diffractive images can be interpreted directly in Fourier space but for most applications real space images are preferable. If the diffractive images are recorded with sufficient detail between the extrema, the phase can be in principle reconstructed.[22] It took until 1999 for the first experimental demonstration of the oversampling method and phase retrieval algorithms to transform diffraction images back to real space.[23] These developments paved the way for coherent diffraction imaging, first at synchrotron radiation light sources and then for XFEL-based single-particle imaging.

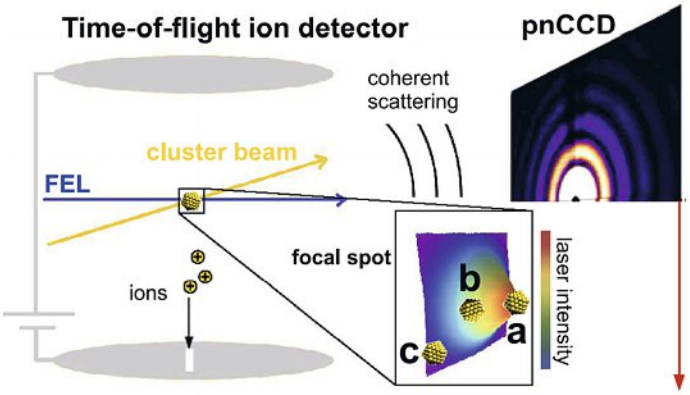

Fig. 5. Layout of a coincidence imaging and spectroscopy experiment. The ion time-of-flight mass spectra and coherent image provide complementary information about the target sample. Image reproduced with permission from ref. [19].

Another famous way to solve the phase problem is holography. Here, the object wave and an additional reference wave interfer with each other. The detector records the interference patterns and hereby the phase is encoded. Multiple types of holography have been developed in the microscopy community. In a first holography setup for free-flying, single particles of a weakly scattering virus was mixed with a strongly scattering xenon cluster reference object.[24] The resulting interference pattern allowed for real space reconstruction of the virus with quality that was at least comparable to the phase retrieval methods.

Both, the phase retrieval as well as the holography approach, have requirements at the data quality that cannot always be matched by the experiments. In these situations the forward simulation approach has proven useful. A real space model is developed, Fourier transformed and compared to the diffractive image.[25,26] The real space model is then adjusted iteratively until at least qualitative agreement is obtained.

2.2 *Imaging Fragile Systems*

Ultrafast x-ray imaging provides unique opportunities for fragile nanoscale samples, that are systems that can be altered or even destroyed by contact with the environment. Examples include either weakly bonded nanoparticles, particle aggregates, or metallic clusters that are quickly oxidized. The number of experiments is continously growing and it is not possible to discuss all of them. In the following we present therefore a few selected but in our opinion representative examples.

2.3 *Structure and Morphology of Nanoparticles*

The first images of van der Waals nanoclusters generated in a supersonic expansion were taken in the early days of the FLASH facility.[12] The early images shown in Fig. 6 reveal already some of the basic features. In the left panel, the coherent image of a single, mostly spherical particle can be seen. The middle panel shows a diffraction image of two particles directly attached to each other akin to a double slit experiment and the right panel shows the interference patterns of two clusters separated in space. Already based on these simple observations, significant insight into the cluster generation dynamics in a supersonic expansion could be obtained. It turned out that between 10 and 30% of all clusters showed the previously underestimated twin cluster configuration with two particles in direct contact.[25] When going to more extreme expansion conditions, the resulting particles change from spherical clusters in agreement with monomer addition, to heavily aggregated particles that do not anneal to the spherical ground state any more, to extremely large "hailstone" like particles.[27] The information whether the coagulating clusters reach the spherical ground state as expected from energetic considerations or freeze out in an intermediate non-spherical state was not accessible with previous methods. In a refined approach to simulate weak diffraction signals from nanocluster aggregates, the size and shape of the substructures could be reconstructed revealing subspheres with sizes as different as 130 nm and 20 nm.[26]

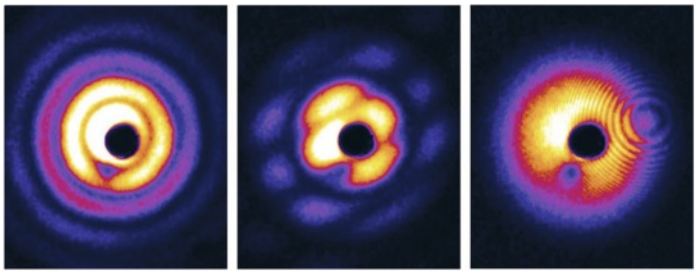

Fig. 6. Some of the first coherent images of van der Waals systems. Single spherical particle (left), distinct interference patterns from two particles next to each other (middle), and separated within the focal volume (right) can be identified. Image reproduced with permission from ref. [12].

Compared to the simple van der Waals systems, metal nanoparticles are known to exhibit much richer growth dynamics, supporting many different and highly symmetric geometries. The investigation of growth processes on the nanoscale can answer key questions on how geometric structure and stability lead to metastable states during particle formation. Single-particle imaging of free and unsupported metal nanoparticles could identify a much larger variety of morphologies on the nanoscale than expected from thermodynamic considerations and preceding ensemble-averaging investigations.[18] A key development for image reconstruction in this study has been the inclusion of wide-angle scattering data and sample absorption effects beyond the first Born approximation. With the new multislice Fourier transform algorithm it was possible to reconstruct the three-dimensional shape of the individual nanoparticles.[18] The left column of Fig. 7 shows the experimental data (top), simulated scattering intensity (middle), as well as reconstructed truncated twinned tetrahedral particle (bottom) with a size of 75 nm. The approach promises to be an efficient tool for future investigations of dynamic processes including melting and phase transitions at the nanoscale.

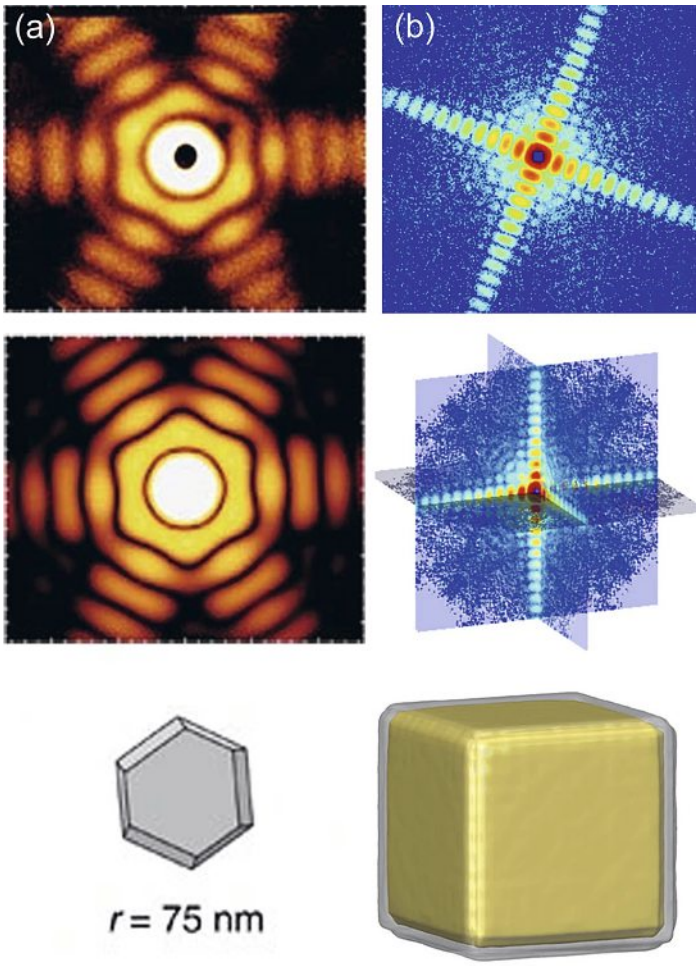

Fig. 7. Coherent images with three dimensional information of metallic nanoparticles. Left: wide angle diffraction image (top), multislice simulation (middle), and reconstructed particle (bottom). Right: Single two-dimensional pattern (top), merged three-dimensional data set (middle), and reconstructed particle (bottom). Images reproduced with permission from ref. [18, 29].

An alternative approach to reconstruct three-dimensional information for highly reproducible or even identical particles is to collect a large amount of randomly orientated two-dimensional diffraction patters that are merged into a three-dimensional data set.[28] In addition, utilizing the high crystallographic symmetry of the sample has also proved to be a promising approach. The right panel of Fig. 7 displays the data for cubic and deposited Au-Pt core-shell particles.[29] The fine-structured single-shot diffraction patterns (top panel) are merged into a diffraction volume (middle panel) and the real space aparticle is reconstructed (bottom panel). The reconstructed particle showed the Au core size and the Pd shell thickness to be 65.0 ± 1.0 nm and 4.0 ± 0.5 nm, respectively, with a resolution of around 6 nm. The data also allowed to describe the elemental distribution inside the nanoparticles with an accuracy of 3%. This approach proves a new way for quantitative 3D imaging of symmetrical nanostructures with elemental specificity.

2.4 *Superfluid He Droplets*

The undoubtably most fragile system investigated by means of single-shot imaging so far are superfluid He droplets, for which the single-shot images allowed a glimpse into the quantum world. Below a critical temperature of 2.17 K the superfluid ^{4}He droplets lack any viscosity and their motion can be described by a single wave function. The initial experiments were motivated by studying the rotational properties and vortices in superfluid droplets on the nanometer to micrometer length scale.[16] In order to visualize the vortices, the droplets are doped with xenon atoms which are known to decorate along them and which act akin to a x-ray contrast agent. The single shot diffraction images reveal distinct Bragg-like diffraction peaks in addition to the droplet envelope. The Bragg patterns indicate that within the droplets highly ordered lattices of quantum vortices are formed that reach densities about five orders of magnitude higher than observed in bulk superfluid ^{4}He experiments.[16] In addition to the quantum vortices, the droplet shape yields information about the rotational speeds of the droplets. The early experiments revealed already strong shape deformations from centrifugal forces, indicating high rotational speeds of the droplets.[16] Following experiments at longer wavelength and exploiting the wide-angle scattering for three dimensional reconstruction, as discussed above, they were able to paint a detailed picture about the shape evolution of superfluid droplets.[30] The data show that also superfluid droplets follow the evolution from axisymmetric oblate to triaxial prolate and two-lobed droplets, similar to their classic counterparts.[30]

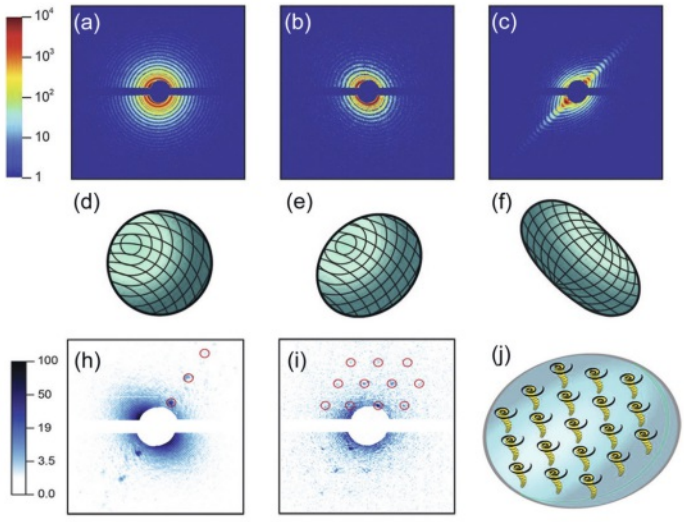

Fig. 8. Coherent images (a-c) and reconstructed shapes (d-f) of superfluid helium droplets. Some images of doped droplets show Bragg-like patterns indicating a high density of ordered quantum vortices (h-j). Image reproduced with permission from ref. [16].

2.5 *Aerosols*

Single-shot single-particle imaging at FELs open new avenues to investigate the size, structure, and composition of aerosols. This approach is particularly interesting for samples that can alter their structure upon deposition as for example soot networks. In a first step on aerosol particles studies at FELs, soot and soot-salt mixtures were investigated with combined imaging and ion time-of-flight spectroscopy. By analyzing the single diffraction patterns and elastic scattering intensity, the fractal morphology of the aggregates is determined. Fig. 9 shows the diffraction patterns and reconstructed particles of sparked-generated soot particle (left) and a salt-soot mixture (right). The size, shape, and electron density

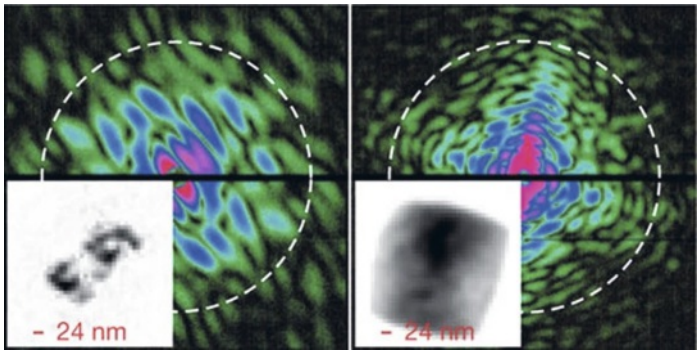

Fig. 9. Coherent diffraction images and real space reconstructions of a spark-generated soot particle (left) and a salt-soot mixture (right). Image reproduced with permission from ref. [21].

can be clearly seen in the reconstructed images. The time-of-flight mass spectra yield additionl information about the elemental composition of each aerosol particle and allows correlations to their shape. This early example demonstrates the opportunities from single-particle imaging for morphological studies or even dynamical processes in aerosol research.

3. Imaging Biological Samples

The potential for ultrafast imaging of biological samples down to single molecules has been one of the early drivers for FEL developments.[2] Already in the very early operational phase of the first hard x-ray laser, much of the biological community focused on serial femtosecond crystallography approaches.[4] Serial crystallogrpahy with jet sources or fixed targets allows the use of smaller crystals, avoids radiation damage, and opens the opportunity to investigate photo-triggered reactions with established crystallographic tools. On the contrary, single-particle imaging of biological samples with the goal of Angstrom resolution requires many dedicated developments,[31] while also facing competition from electron microscopy. Generally, the approach from big to small is followed with first successful experiments on the large Mimi virus with a viral capsid around 450 nm in diameter that is covered by a thin layer of fibers.[32] The high reproducibility of viral targets also allowed the first proof-of-concept demonstration of 3D imaging of a Mimi virus.[33] To collect a series of 2D diffraction patterns of identical copies of the mimivirus, the virus particles were aerosolized, focused, and injected into the intense x-ray pulses. After sorting the data, 198 2D diffraction patterns were analyzed. Fig. 10 shows the assembled 3D diffraction volume and the related real space image of the Mimi virus. The map reveals an asymmetric internal structure and the resolution is still limited to 125 nm, where the limiting factor is the small number of high-quality 2D patterns.

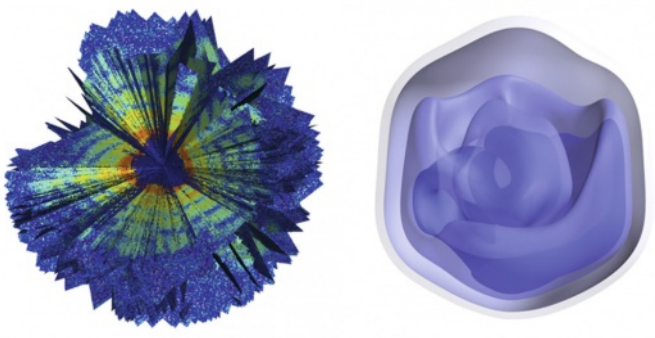

Fig. 10. Merged three-dimensional diffraction data set and real space reconstruction of a Mimi virus. Image reproduced with permission from ref. [33].

The conclusion from the 3D mimivirus reconstruction is consistent with simulation work[34] showing that for a target resolution of around 3 Å of phytochrome molecule, the requirement for good-quality 2D patterns is 672,010 with a photon energy of 6 keV and a high fluence of 10^{20} photons/cm^2. Here, the super-conducting, high-repetition rate FEL sources will make a difference by allowing to collect much richer data sets. The first prototype experiment for high-repetition imaging experiments was carried out at the European-XFEL pushing both the sample size requirements and resolution to much lower values.[35,36] Compared to the Angstrom resolution from cryo-electron microscopy, there is still some way to go for single particle x-ray imaging but the higher penetration depth, the possibility to investigate dynamic processes, and the high throughput can keep single-shot x-ray imaging an attractive option.

4. Imaging Dynamics

The time structure and wavelength of intense soft x-ray FEL pulses are ideally suited to follow ultrafast dynamics on the nanoscale with femtosecond resolution. The ability to image free-flying particles is of particular advantage for nanometer sized samples or processes, where any interaction with a surface could lead to significant distortion either from the pump pulse or the resulting dynamics. In a first study of that kind the expansion of superheated xenon clusters, a prototypical non-equilibrium phenomenon, was investigated.[37] A near-infrared laser pulse was overlaid with the x-ray pulse with a holey mirror where both pulses hit the same target particle with an adjustable time delay as depicted in Fig. 11. The diffraction images show distinct changes starting with a rapid loss of higher order information already within the first 100 femtoseconds that is associated with a surface softening around a solid core. A follow-up study on size-selected SiO_2 particles with better time resolution identified a global start-up delay in the particle expansion dynamics of about 50 fs and could reconstruct the rarefaction wave inside the particles from the coherent particle images.[38] It is noted that the results are in good agreement with hard x-ray Bragg scattering experiments that show that even for superheated clusters the inner core stays crystalline on the femtosecond time scale until the rarefaction wave has traveled from the surface to the particle core.[39] So far, these early examples are driven by high-energy density processes but the results underline nicely the rich information that can also be obtained from time-resolved single-particle imaging applications, opening the door for future applications for photo-triggered reactions in nanoparticles or aerosols.

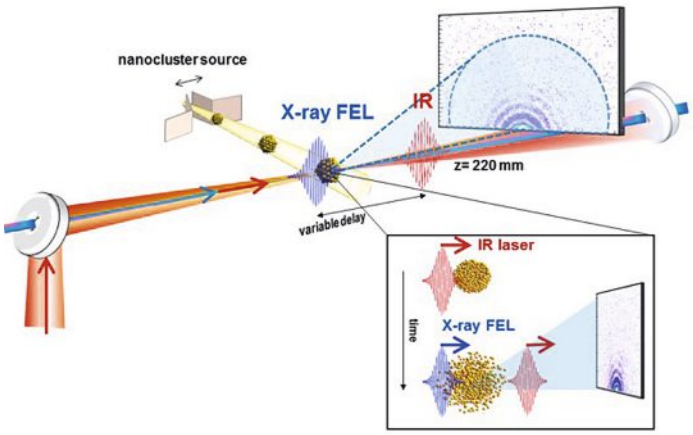

Fig. 11. Setup for imaging the ultrafast dynamics of superheated nanoparticles. Image reproduced with permission from ref. [37].

5. Imaging Electronic Structure

The cross section for elastic scattering is closely related to the electronic structure of the sample. In the fully linear imaging regime this fact has been exploited since a long time for resonantly enhancing contrast of a specific atomic component or by staying below certain resonances. An example for the latter case is water-window imaging of biological specimen where the contrast of carbon is enhanced over oxygen (water) by staying below the oxygen K-edge. Ultrafast imaging experiments open new opportunities in this context as they can become sensitive to either transient resonances or collective electronic excitations. A first indication for transient resonance enhancement of the ultrafast imaging signal was observed from ionic states in xenon clusters.[40] In a subsequent study, resonant scattering revealed distinct core-shell structures in clusters which is attributed to purely electronic effects in otherwise elementally homogenous xenon particles.[41]

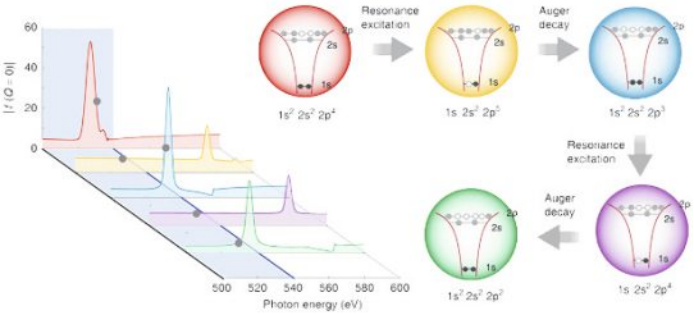

Fig. 12. Calculated x-ray resonances at the oxygen K-edge during the ultrafast imaging process in sucrose nanoparticles. Image reproduced with permission from ref. [42].

The interaction of intense x-ray pulses is highly complex and the discussion has been so far mostly focused on damage processes. A recent combined experimental and theoretical work on dynamic scattering included the excitation and decay processes on the atomic level, showing that transient phenomena driven by non-linear x-ray interaction are decisive for ultrafast imaging applications.[42] Taking sucrose particles as an example, the study showed that around the oxygen K-edge resonance-mediated pathways can lead to multiple Auger cascades as depicted in Fig. 12. Accordingly, the scattering amplitudes and related atomic form factors change rapidly with the different decay channels. While these are so far fundamental studies about the image generation process in intense x-ray pulses, they show potential opportunities how transient resonances may be exploited for increasing the scattering response and elemental or even electronic contrast in diffractive imaging experiments.

6. Growing Opportunities at SwissFEL

The new Maloja endstation at the SwissFEL Athos soft x-ray branch is designed as highly versatile tool for AMO physics, chemical sciences, soft x-ray imaging, and novel approaches in non-linear x-ray spectroscopy. The x-ray pulses are delivered with the minimum required three bounces from a single offset mirror and two Kirkpatrick-Baetz focusing mirrors. A short focal length of 1.5 meters from the downstream KB mirror ensures a tight, micron-sized focus and therefore sufficient fluence for the photon-hungry single-particle imaging experiments while maintaining enough space for laser incoupling elements and differential pumping between the last optical element and the endstation.

The top panel of Fig. 13 shows the conceptual layout of the Maloja endstation. A variety of spectrometer and detector options can be implemented including ion time-of-flight or ion momentum spectrometers, a hemispherical electron analyzer, or a photon spectrometer. The most important detector for the single-particle

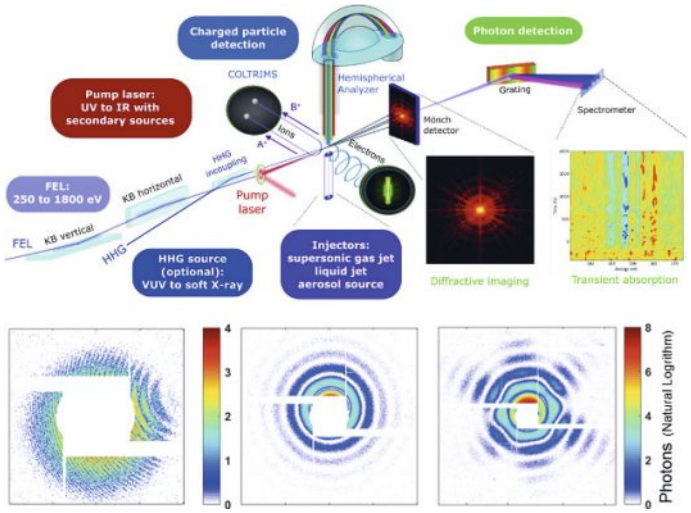

Fig. 13. top: Schematic layout of the new Maloja endstation at SwissFEL. Bottom: First diffraction images from the Maloja endstation commissioning phase from xenon (left), polystyrene (middle), as well as gold (right) nanoparticles.

imaging research program is a 4 MPixel Jungfrau pixel detector optimized for soft x-ray photon detection.[14] The bottom panel of Fig. 13 displays three diffraction images with the interference pattern of two xenon clusters, a 92 nm polystyrene particle, and a 58 nm gold nanoparticle. Compared to the early diffraction images in Fig. 6, the advances in detector technology and dynamic range are particular obvious. For the imaging setup, a supersonic expansion source and an aerosol injector system are available allowing to extend the ultrafast imaging capabilities to a wide spectrum of chemical and biological systems. The Maloja endstation in combination with ultrafast optical laser-driven sources and the unique pulse characteristics from the Athos undulator will enable new approaches in non-linear x-ray sciences and ultrafast imaging.

7. Conclusions

Ultrafast single-particle imaging with intense x-ray pulses is a new and powerful tool to visualize structure and dynamics on the nanoscale. First applications range from nanoparticle morphology and growth dynamics to the behavior of superfluid nanodroplets to biological systems and aerosol research. Current developments push the field towards time-resolved imaging of ultrafast dynamics and imaging of transient electronic structure. The new Maloja endstation at SwissFEL promises new opportunities for ultrafast spectroscopy and imaging for the chemical, physical, and biological research community.

Acknowledgements

The Maloja instrument received funding from the Swiss National Science Foundation through R'Equip Grant No. 206021_182988. Zhibin Sun acknowledges a Marie Skłodowska–Curie Grant funded by the European Union's Horizon 2020 research and innovation program under contract no. 701647.

Received: May 15, 2022

[1] C. Pellegrini, A. Marinelli, S. Reiche, *Rev. Mod. Phys.* **2016**, *88*, 015006, https://doi.org/10.1103/RevModPhys.88.015006.

[2] R. Neutze, R. Wouts, D. Spoel, E. Weckert, J. Hajdu, *Nature* **2000**, *406,* 752, https://doi.org/10.1038/35021099.

[3] H. N. Chapman, A. Barty, M. J. Bogan, S. Boutet, M. Frank, S. P. Hau-Riege, S. Marchesini, B. W. Woods, S. Bajt, W. H. Benner, R. A. London, E. Plonjes, M. Kuhlmann, R. Treusch, S. Dusterer, T. Tschentscher, J. R. Schneider, E. Spiller, T. Moller, C. Bostedt, M. Hoener, D. A. Shapiro, K. O. Hodgson, D. van der Spoel, F. Burmeister, M. Bergh, C. Caleman, G. Huldt, M. M. Seibert, F. R. N. C. Maia, R. W. Lee, A. Szoke, N. Timneanu, J. Hajdu, *Nat. Phys.* **2006**, *2*, 839, https://doi.org/10.1038/nphys461.

[4] C. Bostedt, S. Boutet, D. M. Fritz, Z. Huang, H. J. Lee, H. T. Lemke, A. Robert, W. F. Schlotter, J. J. Turner, G. J. Williams, *Rev. Mod. Phys.* **2016**, *88,* 015007, https://doi.org/10.1103/RevModPhys.88.015007.

[5] J. Duris, S. Li, T. Driver, E. G. Champenois, J. P. MacArthur, A. A. Lutman, Z. Zhang, P. Rosenberger, J. W. Aldrich, R. Coffee, G. Coslovich, F.-J. Decker, J. M. Glownia, G. Hartmann, W. Helml, A. Kamalov, J. Knurr, J. Krzywinski, M.-F. Lin, J. P. Marangos, M. Nantel, A. Natan, J. T. O'Neal, N. Shivaram, P. Walter, A. L. Wang, J. J. Welch, T. J. A. Wolf, J. Z. Xu, M. F. Kling, P. H. Bucksbaum, A. Zholents, Z. Huang, J. P. Cryan, A. Marinelli, *Nat. Photonics* **2020**, *14*, 30, https://doi.org/10.1038/s41566-019-0549-5.

[6] A. A. Lutman, T. J. Maxwell, J. P. MacArthur, M. W. Guetg, N. Berrah, R. N. Coffee, Y. Ding, Z. Huang, A. Marinelli, S. Moeller, J. C. U. Zemella, *Nat. Photonics* **2016**, *10*, 745, https://doi.org/10.1038/nphoton.2016.201.

[7] E. Prat, P. Dijkstal, E. Ferrari, R. Ganter, P. Juranić, A. Malyzhenkov, S. Reiche, T. Schietinger, G. Wang, A. A. Haddad, S. Augustin, C. Bostedt, G. Knopp, J. Knurr, A. S. Morillo-Candas, Z. Sun, K. Schnorr, *Phys. Rev. Research* **2022**, *4*, L022025, https://doi.org/10.1103/PhysRevResearch.4.L022025.

[8] P. Willmott. *An Introduction to Synchrotron Radiation: Techniques and Applications*, 2nd edn, John Wiley & Sons, Inc., **2019**, ISBN: 978-1-119-28039-2.

[9] E. Prat, R. Abela, M. Aiba, A. Alarcon, J. Alex, Y. Arbelo, C. Arrell, V. Arsov, C. Bacellar, C. Beard, P. Beaud, S. Bettoni, R. Biffiger, M. Bopp, H.-H. Braun, M. Calvi, A. Cassar, T. Celcer, M. Chergui, P. Chevtsov, C. Cirelli, A. Citterio, P. Craievich, M. C. Divall, A. Dax, M. Dehler, Y. Deng, A. Dietrich, P. Dijkstal, R. Dinapoli, S. Dordevic, S. Ebner, D. Engeler, C. Erny, V. Esposito, E. Ferrari, U. Flechsig, R. Follath, F. Frei, R. Ganter, T. Garvey, Z. Geng, A. Gobbo, C. Gough, A. Hauff, C. P. Hauri, N. Hiller, S. Hunziker, M. Huppert, G. Ingold, R. Ischebeck, M. Janousch, P. J. M. Johnson, S. L. Johnson, P. Juranić, M. Jurcevic, M. Kaiser, R. Kalt, B. Keil, D. Kiselev, C. Kittel, G. Knopp, W. Koprek, M. Laznovsky, H. T. Lemke, D. L. Sancho, F. Löhl, A. Malyzhenkov, G. F. Mancini, R. Mankowsky, F. Marcellini, G. Marinkovic, I. Martiel, F. Märki, C. J. Milne, A. Mozzanica, K. Nass, G. L. Orlandi, C. O. Loch, M. Paraliev, B. Patterson, L. Patthey, B. Pedrini, M. Pedrozzi, C. Pradervand, P. Radi, J.-Y. Raguin, S. Redford, J. Rehanek, S. Reiche, L. Rivkin, A. Romann, L. Sala, M. Sander, T. Schietinger, T. Schilcher, V. Schlott, T. Schmidt, M. Seidel, M. Stadler, L. Stingelin, C. Svetina, D. M. Treyer, A. Trisorio, C. Vicario, D. Voulot, A. Wrulich, S. Zerdane, E. Zimoch, *Nat. Photonics* **2020**, *14*, 748, https://doi.org/10.1038/s41566-020-00712-8.

[10] E. Prat, M. Calvi, S. Reiche, *J. Synchrotron Rad.* **2016**, *23*, 874, https://doi.org/10.1107/S1600577516007177.

[11] R. Abela, A. Alarcon, J. Alex, C. Arrell, V. Arsov, S. Bettoni, M. Bopp, C. Bostedt, H.-H. Braun, M. Calvi, T. Celcer, P. Craievich, A. Dax, P. Dijkstal, S. Dordevic, E. Ferrari, U. Flechsig, R. Follath, F. Frei, N. Gaiffi, Z. Geng, C. Gough, N. Hiller, S. Hunziker, M. Huppert, R. Ischebeck, H. Johri, P. Juranic, R. Kalt, M. Kaiser, B. Keil, C. Kittel, R. Kunzi, T. Lippuner, F. Lohl, F. Marcellini, G. Marinkovic, C. Ozkan Loch, G. L. Orlandi, B. Patterson, C. Pradervand, M. Paraliev, M. Pedrozzi, E. Prat, P. Ranitovic, S. Reiche, C. Rosenberg, S. Sanfilippo, T. Schietinger, T. Schmidt, K. Schnorr, C. Svetina, A. Trisorio, C. Vicario, D. Voulot, U. Wagner, H. J. Worner, A. Zandonella, L. Patthey, R. Ganter, *J. Synchrotron Rad.* **2019**, *26*, 1073, https://doi.org/10.1107/S1600577519003928.

[12] C. Bostedt, M. Adolph, E. Eremina, M. Hoener, D. Rupp, S. Schorb, H. Thomas, A. R. B. de Castro, T. Möller, *J. Phys. B: At., Mol. Opt. Phys.* **2010**, *43*, 194011, https://doi.org/10.1088/0953-4075/43/19/194011.

[13] L. Strüder, S. Epp, D. Rolles, R. Hartmann, P. Holl, G. Lutz, H. Soltau, R. Eckart, C. Reich, K. Heinzinger, C. Thamm, A. Rudenko, F. Krasniqi, K.-U. Kühnel, C. Bauer, C.-D. Schröter, R. Moshammer, S. Techert, D. Miessner, M. Porro, O. Hälker, N. Meidinger, N. Kimmel, R. Andritschke, F. Schopper, G. Weidenspointner, A. Ziegler, D. Pietschner, S. Herrmann, U. Pietsch, A. Walenta, W. Leitenberger, C. Bostedt, T. Möller, D. Rupp, M. Adolph, H. Graafsma, H. Hirsemann, K. Gärtner, R. Richter, L. Foucar, R. L. Shoeman, I. Schlichting, J. Ullrich, *Nucl. Instrum. Methods Phys. Res. A* **2010**, *614*, 483, https://doi.org/10.1016/j.nima.2009.12.053.

[14] A. Mozzanica, M. Andrä, R. Barten, A. Bergamaschi, S. Chiriotti, M. Brückner, R. Dinapoli, E. Fröjdh, D. Greiffenberg, F. Leonarski, C. Lopez-Cuenca, D. Mezza, S. Redford, C. Ruder, B. Schmitt, X. Shi, D. Thattil, G. Tinti, S. Vetter, J. Zhang, *Synchrotron Radiat. News* **2018**, *31*, 16, https://doi.org/10.1080/08940886.2018.1528429.

[15] Z. Sun, J. Fan, H. Li, H. Liu, D. Nam, C. Kim, Y. Kim, Y. Han, J. Zhang, S. Yao, J. Park, S. Kim, K. Tono, M. Yabashi, T. Ishikawa, C. Song, C. Fan, H. Jiang, *ACS Nano* **2018**, *12*, 7509, https://doi.org/10.1021/acsnano.8b01838.

[16] L. F. Gomez, K. R. Ferguson, J. P. Cryan, C. Bacellar, R. M. P. Tanyag, C. Jones, S. Schorb, D. Anielski, A. Belkacem, C. Bernando, R. Boll,

J. Bozek, S. Carron, G. Chen, T. Delmas, L. Englert, S. W. Epp, B. Erk, L. Foucar, R. Hartmann, A. Hexemer, M. Huth, J. Kwok, S. R. Leone, J. H. S. Ma, F. R. N. C. Maia, E. Malmerberg, S. Marchesini, D. M. Neumark, B. Poon, J. Prell, D. Rolles, B. Rudek, A. Rudenko, M. Seifrid, K. R. Siefermann, F. P. Sturm, M. Swiggers, J. Ullrich, F. Weise, P. Zwart, C. Bostedt, O. Gessner, A. F. Vilesov, *Science* **2014**, *345*, 906, https://doi.org/10.1126/science.1252395.

[17] J. Bielecki, M. F. Hantke, B. J. Daurer, H. K. N. Reddy, D. Hasse, D. S. D. Larsson, L. H. Gunn, M. Svenda, A. Munke, J. A. Sellberg, L. Flueckiger, A. Pietrini, C. Nettelblad, I. Lundholm, G. Carlsson, K. Okamoto, N. Timneanu, D. Westphal, O. Kulyk, A. Higashiura, G. v. d. Schot, N.-T. D. Loh, T. E. Wysong, C. Bostedt, T. Gorkhover, B. Iwan, M. M. Seibert, T. Osipov, P. Walter, P. Hart, M. Bucher, A. Ulmer, D. Ray, G. Carini, K. R. Ferguson, I. Andersson, J. Andreasson, J. Hajdu, F. R. N. C. Maia, *Sci. Adv.* **2019**, *5*, eaav8801, https://doi.org/10.1126/sciadv.aav8801.

[18] I. Barke, H. Hartmann, D. Rupp, L. Flückiger, M. Sauppe, M. Adolph, S. Schorb, C. Bostedt, R. Treusch, C. Peltz, S. Bartling, T. Fennel, K.-H. Meiwes-Broer, T. Möller, *Nat. Commun.* **2015**, *6,* 6187, https://doi.org/10.1038/ncomms7187.

[19] T. Gorkhover, M. Adolph, D. Rupp, S. Schorb, S. W. Epp, B. Erk, L. Foucar, R. Hartmann, N. Kimmel, K. U. Kühnel, D. Rolles, B. Rudek, A. Rudenko, R. Andritschke, A. Aquila, J. D. Bozek, N. Coppola, T. Erke, F. Filsinger, H. Gorke, H. Graafsma, L. Gumprecht, G. Hauser, S. Herrmann, H. Hirsemann, A. Hömke, P. Holl, C. Kaiser, F. Krasniqi, J. H. Meyer, M. Matysek, M. Messerschmidt, D. Miessner, B. Nilsson, D. Pietschner, G. Potdevin, C. Reich, G. Schaller, C. Schmidt, F. Schopper, C. D. Schröter, J. Schulz, H. Soltau, G. Weidenspointner, I. Schlichting, L. Strüder, J. Ullrich, T. Möller, C. Bostedt, *Phys. Rev. Lett.* **2012**, *108*, 245005, https://doi.org/10.1103/PhysRevLett.108.245005.

[20] H. Thomas, C. Bostedt, M. Hoener, E. Eremina, H. Wabnitz, T. Laarmann, E. Plönjes, R. Treusch, A. R. B. de Castro, T. Möller, *J. Phys. B: At., Mol. Opt. Phys.* **2009**, *42*, 134018, https://doi.org/10.1088/0953-4075/42/13/134018.

[21] N. D. Loh, C. Y. Hampton, A. V. Martin, D. Starodub, R. G. Sierra, A. Barty, A. Aquila, J. Schulz, L. Lomb, J. Steinbrener, R. L. Shoeman, S. Kassemeyer, C. Bostedt, J. Bozek, S. W. Epp, B. Erk, R. Hartmann, D. Rolles, A. Rudenko, B. Rudek, L. Foucar, N. Kimmel, G. Weidenspointner, G. Hauser, P. Holl, E. Pedersoli, M. Liang, M. S. Hunter, L. Gumprecht, N. Coppola, C. Wunderer, H. Graafsma, F. R. N. C. Maia, T. Ekeberg, M. Hantke, H. Fleckenstein, H. Hirsemann, K. Nass, T. A. White, H. J. Tobias, G. R. Farquar, W. H. Benner, S. P. Hau-Riege, C. Reich, A. Hartmann, H. Soltau, S. Marchesini, S. Bajt, M. Barthelmess, P. Bucksbaum, K. O. Hodgson, L. Strüder, J. Ullrich, M. Frank, I. Schlichting, H. N. Chapman, M. J. Bogan, *Nature* **2012**, *486*, 513, https://doi.org/10.1038/nature11222.

[22] J. R. Fienup, *Appl. Opt.* **1982**, *21*, 2758, https://doi.org/10.1364/AO.21.002758.

[23] J. Miao, P. Charalambous, J. Kirz, D. Sayre, *Nature* **1999**, *400*, 342, https://doi.org/10.1038/22498.

[24] T. Gorkhover, A. Ulmer, K. Ferguson, M. Bucher, F. R. N. C. Maia, J. Bielecki, T. Ekeberg, M. F. Hantke, B. J. Daurer, C. Nettelblad, J. Andreasson, A. Barty, P. Bruza, S. Carron, D. Hasse, J. Krzywinski, D. S. D. Larsson, A. Morgan, K. Mühlig, M. Müller, K. Okamoto, A. Pietrini, D. Rupp, M. Sauppe, G. van der Schot, M. Seibert, J. A. Sellberg, M. Svenda, M. Swiggers, N. Timneanu, D. Westphal, G. Williams, A. Zani, H. N. Chapman, G. Faigel, T. Möller, J. Hajdu, C. Bostedt, *Nat. Photonics* **2018**, *12*, 150, https://doi.org/10.1038/s41566-018-0110-y.

[25] D. Rupp, M. Adolph, T. Gorkhover, S. Schorb, D. Wolter, R. Hartmann, N. Kimmel, C. Reich, T. Feigl, A. R. B. de Castro, R. Treusch, L. Strüder, T. Möller, C. Bostedt, *New J. Phys.* **2012**, *14,* 055016, https://doi.org/10.1088/1367-2630/14/5/055016.

[26] T. Nishiyama, A. Niozu, C. Bostedt, K. R. Ferguson, Y. Sato, C. Hutchison, K. Nagaya, H. Fukuzawa, K. Motomura, S.-i. Wada, T. Sakai, K. Matsunami, K. Matsuda, T. Tachibana, Y. Ito, W. Xu, S. Mondal, T. Umemoto, C. Nicolas, C. Miron, T. Kameshima, Y. Joti, K. Tono, T. Hatsui, M. Yabashi, K. Ueda, *IUCrJ* **2020**, *7*, 10, https://doi.org/10.1107/S2052252519014222.

[27] D. Rupp, M. Adolph, L. Flückiger, T. Gorkhover, J. P. Müller, M. Müller, M. Sauppe, D. Wolter, S. Schorb, R. Treusch, C. Bostedt, T. Möller, *J. Chem. Phys.* **2014**, *141*, 044306, https://doi.org/10.1063/1.4890323.

[28] K. Ayyer, P. L. Xavier, J. Bielecki, Z. Shen, B. J. Daurer, A. K. Samanta, S. Awel, R. Bean, A. Barty, M. Bergemann, T. Ekeberg, A. D. Estillore, H. Fangohr, K. Giewekemeyer, M. S. Hunter, M. Karnevskiy, R. A. Kirian, H. Kirkwood, Y. Kim, J. Koliyadu, H. Lange, R. Letrun, J. Lübke, T. Michelat, A. J. Morgan, N. Roth, T. Sato, M. Sikorski, F. Schulz, J. C. H. Spence, P. Vagovic, T. Wollweber, L. Worbs, O. Yefanov, Y. Zhuang, F. R. N. C. Maia, D. A. Horke, J. Küpper, N. D. Loh, A. P. Mancuso, H. N. Chapman, *Optica* **2021**, *8*, 15, https://doi.org/10.1364/OPTICA.410851.

[29] A. Pryor, A. Rana, R. Xu, J. A. Rodriguez, Y. Yang, M. Gallagher-Jones, H. Jiang, K. Kanhaiya, M. Nathanson, J. Park, S. Kim, S. Kim, D. Nam, Y. Yue, J. Fan, Z. Sun, B. Zhang, D. F. Gardner, C. S. B. Dias, Y. Joti, T. Hatsui, T. Kameshima, Y. Inubushi, K. Tono, J. Y. Lee, M. Yabashi, C. Song, T. Ishikawa, H. C. Kapteyn, M. M. Murnane, H. Heinz, J. Miao, *Sci. Rep.* **2018**, *8*, 8284, https://doi.org/10.1038/s41598-018-26182-1.

[30] B. Langbehn, K. Sander, Y. Ovcharenko, C. Peltz, A. Clark, M. Coreno, R. Cucini, M. Drabbels, P. Finetti, M. Di Fraia, L. Giannessi, C. Grazioli, D. Iablonskyi, A. C. LaForge, T. Nishiyama, V. Oliver Álvarez de Lara, P. Piseri, O. Plekan, K. Ueda, J. Zimmermann, K. C. Prince, F. Stienkemeier, C. Callegari, T. Fennel, D. Rupp, T. Möller, *Phys. Rev. Lett.* **2018**, *121*, 255301, https://doi.org/10.1103/PhysRevLett.121.255301.

[31] A. Aquila, A. Barty, C. Bostedt, S. Boutet, G. Carini, D. dePonte, P. Drell, S. Doniach, K. H. Downing, T. Earnest, H. Elmlund, V. Elser, M. Gühr, J. Hajdu, J. Hastings, S. P. Hau-Riege, Z. Huang, E. E. Lattman, F. R. N. C. Maia, S. Marchesini, A. Ourmazd, C. Pellegrini, R. Santra, I. Schlichting, C. Schroer, J. C. H. Spence, I. A. Vartanyants, S. Wakatsuki, W. I. Weis, G. J. Williams, *Struct. Dyn.* **2015**, *2*, 041701, https://doi.org/10.1063/1.4918726.

[32] M. M. Seibert, T. Ekeberg, F. R. N. C. Maia, M. Svenda, J. Andreasson, O. Jonsson, D. Odic, B. Iwan, A. Rocker, D. Westphal, M. Hantke, D. P. DePonte, A. Barty, J. Schulz, L. Gumprecht, N. Coppola, A. Aquila, M. Liang, T. A. White, A. Martin, C. Caleman, S. Stern, C. Abergel, V. Seltzer, J.-M. Claverie, C. Bostedt, J. D. Bozek, S. Boutet, A. A. Miahnahri, M. Messerschmidt, J. Krzywinski, G. Williams, K. O. Hodgson, M. J. Bogan, C. Y. Hampton, R. G. Sierra, D. Starodub, I. Andersson, S. Bajt, M. Barthelmess, J. C. H. Spence, P. Fromme, U. Weierstall, R. Kirian, M. Hunter, R. B. Doak, S. Marchesini, S. P. Hau-Riege, M. Frank, R. L. Shoeman, L. Lomb, S. W. Epp, R. Hartmann, D. Rolles, A. Rudenko, C. Schmidt, L. Foucar, N. Kimmel, P. Holl, B. Rudek, B. Erk, A. Homke, C. Reich, D. Pietschner, G. Weidenspointner, L. Struder, G. Hauser, H. Gorke, J. Ullrich, I. Schlichting, S. Herrmann, G. Schaller, F. Schopper, H. Soltau, K.-U. Kuhnel, R. Andritschke, C.-D. Schroter, F. Krasniqi, M. Bott, S. Schorb, D. Rupp, M. Adolph, T. Gorkhover, H. Hirsemann, G. Potdevin, H. Graafsma, B. Nilsson, H. N. Chapman, J. Hajdu, *Nature* **2011**, *470*, 78,

[33] T. Ekeberg, M. Svenda, C. Abergel, F. R. N. C. Maia, V. Seltzer, J.-M. Claverie, M. Hantke, O. Jönsson, C. Nettelblad, G. Van Der Schot, *Phys. Rev. Lett.* **2015**, *114*, 098102, https://doi.org/10.1103/PhysRevLett.114.098102.

[34] I. Poudyal, M. Schmidt, P. Schwander, *truct. Dyn.* **2020**, *7*, 024102, https://doi.org/10.1063/1.5144516.

[35] E. Sobolev, S. Zolotarev, K. Giewekemeyer, J. Bielecki, K. Okamoto, H. K. N. Reddy, J. Andreasson, K. Ayyer, I. Barak, S. Bari, A. Barty, R. Bean, S. Bobkov, H. N. Chapman, G. Chojnowski, B. J. Daurer, K. Dörner, T. Ekeberg, L. Flückiger, O. Galzitskaya, L. Gelisio, S. Hauf, B. G. Hogue, D. A. Horke, A. Hosseinizadeh, V. Ilyin, C. Jung, C. Kim, Y. Kim, R. A. Kirian, H. Kirkwood, O. Kulyk, J. Küpper, R. Letrun, N. D. Loh, K. Lorenzen, M. Messerschmidt, K. Mühlig, A. Ourmazd, N. Raab, A. V. Rode, M. Rose, A. Round, T. Sato, R. Schubert, P. Schwander, J. A. Sellberg, M. Sikorski, A. Silenzi, C. Song, J. C. H. Spence, S. Stern, J. Sztuk-Dambietz, A. Teslyuk, N. Timneanu, M. Trebbin, C. Uetrecht, B. Weinhausen, G. J. Williams, P. L. Xavier, C. Xu, I. A. Vartanyants, V. S. Lamzin, A. Mancuso, F. R. N. C. Maia, *Commun. Phys.* **2020**, *3,* 97, https://doi.org/10.1038/s42005-020-0362-y.

[36] T. Ekeberg, D. Assalauova, J. Bielecki, R. Boll, B. J. Daurer, L. A. Eichacker, L. E. Franken, D. E. Galli, L. Gelisio, L. Gumprecht, L. H. Gunn, J. Hajdu, R. Hartmann, D. Hasse, A. Ignatenko, J. Koliyadu, O. Kulyk, R. Kurta, M. Kuster, W. Lugmayr, J. Lübke, A. P. Mancuso, T. Mazza, C. Nettelblad, Y. Ovcharenko, D. E. Rivas, M. Rose, A. K. Samanta, P. Schmidt, E. Sobolev, N. Timneanu, S. Usenko, D. Westphal, T. Wollweber, L. Worbs, P. L. Xavier, H. Yousef, K. Ayyer, H. N. Chapman, J. A. Sellberg, C. Seuring, I. A. Vartanyants, J. Küpper, M. Meyer, F. R. N. C. Maia, *bioRxiv* **2022**, 483477,

[37] T. Gorkhover, S. Schorb, R. Coffee, M. Adolph, L. Foucar, D. Rupp, A. Aquila, J. D. Bozek, S. W. Epp, B. Erk, L. Gumprecht, L. Holmegaard, A. Hartmann, R. Hartmann, G. Hauser, P. Holl, A. Hömke, P. Johnsson, N. Kimmel, K.-U. Kühnel, M. Messerschmidt, C. Reich, A. Rouzée, B. Rudek, C. Schmidt, J. Schulz, H. Soltau, S. Stern, G. Weidenspointner, B. White, J. Küpper, L. Strüder, I. Schlichting, J. Ullrich, D. Rolles, A. Rudenko, T. Möller, C. Bostedt, *Nat. Photonics* **2016**, *10*, 93, https://doi.org/10.1038/nphoton.2015.264.

[38] C. Peltz, J. A. Powell, P. Rupp, A. Summers, T. Gorkhover, M. Gallei, I. Halfpap, E. Antonsson, B. Langer, C. Trallero-Herrero, C. Graf, D. Ray, Q. Liu, T. Osipov, M. Bucher, K. Ferguson, S. Möller, S. Zherebtsov, D. Rolles, E. Rühl, G. Coslovich, R. N. Coffee, C. Bostedt, A. Rudenko, M. F. Kling, T. Fennel, *New J. Phys.* **2022**, *24*, 043024, https://doi.org/10.1088/1367-2630/ac5e86.

[39] T. Nishiyama, Y. Kumagai, A. Niozu, H. Fukuzawa, K. Motomura, M. Bucher, Y. Ito, T. Takanashi, K. Asa, Y. Sato, D. You, Y. Li, T. Ono, E. Kukk, C. Miron, L. Neagu, C. Callegari, M. Di Fraia, G. Rossi, D. E. Galli, T. Pincelli, A. Colombo, T. Kameshima, Y. Joti, T. Hatsui, S. Owada, T. Katayama, T. Togashi, K. Tono, M. Yabashi, K. Matsuda, C. Bostedt, K. Nagaya, K. Ueda, *Phys. Rev. Lett.* **2019**, *123*, 123201, https://doi.org/10.1103/PhysRevLett.123.123201.

[40] C. Bostedt, E. Eremina, D. Rupp, M. Adolph, H. Thomas, M. Hoener, A. R. B. de Castro, J. Tiggesbäumker, K. H. Meiwes-Broer, T. Laarmann, H. Wabnitz, E. Plönjes, R. Treusch, J. R. Schneider, T. Möller, *Phys. Rev. Lett.* **2012**, *108*, 093401, https://doi.org/10.1103/PhysRevLett.108.093401.

[41] D. Rupp, L. Flückiger, M. Adolph, A. Colombo, T. Gorkhover, M. Harmand, M. Krikunova, J. P. Müller, T. Oelze, Y. Ovcharenko, M. Richter, M. Sauppe,

S. Schorb, R. Treusch, D. Wolter, C. Bostedt, T. Möller, *Struct. Dyn.* **2020**, *7*, 034303, https://doi.org/10.1063/4.0000006.

[42] P. J. Ho, B. J. Daurer, M. F. Hantke, J. Bielecki, A. Al Haddad, M. Bucher, G. Doumy, K. R. Ferguson, L. Flückiger, T. Gorkhover, B. Iwan, C. Knight, S. Moeller, T. Osipov, D. Ray, S. H. Southworth, M. Svenda, N. Timneanu, A. Ulmer, P. Walter, J. Hajdu, L. Young, F. R. N. C. Maia, C. Bostedt, *Nat. Commun.* **2020**, *11*, 167, https://doi.org/10.1038/s41467-019-13905-9.

License and Terms

The definitive version of this article is the electronic one that can be found at https://doi.org/10.2533/chimia.2022.529